Journal of Materials Processing Tech. 255 (2018) 195–203

Contents lists available at ScienceDirect

Journal of Materials Processing Tech.

journal homepage: www.elsevier.com/locate/jmatprotec

Microstructure and mechanical properties of C_f/Al-TiAl laser-assisted brazed joint

Guangjie Feng[a,b], Zhuoran Li[a,*], Zhi Zhou[a], Yong Yang[b], Dusan P. Sekulic[a,d], Michael R. Zachariah[b,c]

[a] State Key Laboratory of Advanced Welding and Joining, Harbin Institute of Technology, Harbin 150001, China
[b] Department of Chemical and Biomolecular Engineering, University of Maryland, College Park, MD 20742, USA
[c] Department of Chemistry and Biochemistry, University of Maryland, College Park, MD 20742, USA
[d] Department of Mechanical Engineering, College of Engineering, University of Kentucky, Lexington, KY 40506, USA

ARTICLE INFO

Keywords:
C_f/Al composites
TiAl alloys
Brazing
Self-propagating high-temperature synthesis
Mechanical properties
Microstructures

ABSTRACT

A high-efficiency brazing method was developed to join C_f/Al composites to TiAl alloys with the assistance of laser-induced exothermic reaction of a Ni-Al-Zr interlayer. The microstructure and mechanical properties of the C_f/Al-TiAl joint were investigated. The joint interfacial structure represented TiAl alloys/Al_3NiTi_2/NiAl + Ni-Al-Zr + Al-Cu-Ti + Ag(s,s)/(Ni,Ti,Zr)Al_3/C_f/Al composites. A ~ 400 nm thick Ti and Zr rich layer was formed around carbon fibers, largely enhancing the bonding quality on the C_f/Al side. The thickness of AgCu foils on each side and the brazing pressure influenced the interfacial reactions and the joint morphology. When the thickness of AgCu foils was 100 μm and the brazing pressure was 4 MPa, the joint was free of defects, and had a maximum shear strength of 71.6 MPa.

1. Introduction

Carbon fiber reinforced aluminum matrix composites (C_f/Al) feature (i) low density, (ii) high specific strength and stiffness, as well as (iii) good structural stability in a variety of environments. Pai et al. (2015) and Velamati et al. (2012) reported that C_f/Al composites have been successfully applied on waveguide tube and antenna frame on satellites, as well as aircraft skin components. TiAl alloys exhibit favorable features such as high creep and oxidation resistance at elevated temperatures according to the studies by Zhao et al. (2016) and Cheng et al. (2016). Due to their excellent performances, these two materials are regarded as the promising aerospace materials. In aerospace field, to reduce weight and achieve combined advantages, partially substituting C_f/Al composites and TiAl alloys to produce composite structures is an effective method. The reliable joining of C_f/Al composites to TiAl alloys is of great meaning, thereby promoting a potential for more applications and bringing sizable technological as well as economic benefits.

Feng et al. (2015a,b,c) and Li et al. (2015, 2016) reported that fusion welding, friction welding and diffusion bonding would damage the connection between reinforced fibers and aluminum matrix, thus degrading the properties of C_f/Al composites. Although brazing was the most feasible technique for joining dissimilar materials, as suggested by Cao et al. (2017) and Song et al. (2017), few studies have been reported on brazing C_f/Al composites to other materials (e.g., TiAl alloys). A lack of appropriate filler metal is the key problem. In brazing aluminum composites, Al-based filler metal is the first choice. But when the TiAl was brazed using Al-based filler metal by Shiue et al. (2003), a brittle $TiAl_3$ layer was formed within the joint domain, seriously affecting the bond quality. Dai et al. (2015) brazed TiAl/ZrO_2 using Ag–Cu filler metal. They preferred AgCu filler metal in brazing TiAl alloys since it can relieve the Coefficient of Thermal Expansion (CTE) mismatch of involved dissimilar materials. Song et al. (2017), Li et al. (2008) and Cao et al. (2011) also brazed TiAl alloys using Ti-Ni, Ti-Si and Ti-Ni-Si filler metals respectively. One main problem of these filler metals is that their high melting points, which excludes the possible application in brazing aluminum composites. Up to now, very few good solutions to this issue have been given.

The Self-propagating High-temperature Synthesis (SHS) technique provides another alternative to solve this problem. The application of SHS in brazing field has unique advantages. After being ignited, it can provide sufficient heat and serve as a local high-temperature source for joining process. The AgCu filler metal or active filler metal (containing Ti, Zr or Ni), which have higher melting points than aluminum matrix, can be rapidly melted without overheating the aluminum composites. SHS assisted brazing can also be high-efficiency (only need a few seconds) since it avoids the long-time heating in vacuum furnace. Pascal

* Corresponding author.
E-mail address: lizr@hit.edu.cn (Z. Li).

https://doi.org/10.1016/j.jmatprotec.2017.12.017
Received 27 October 2017; Received in revised form 10 December 2017; Accepted 11 December 2017
Available online 12 December 2017
0924-0136/

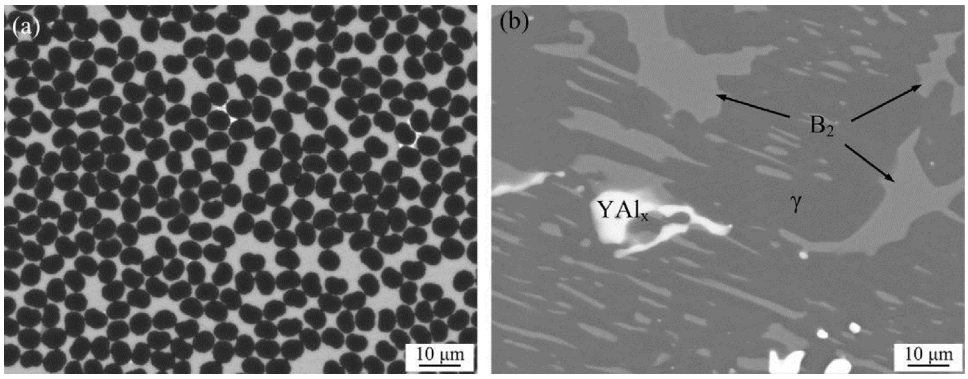

Fig. 1. Microstructures of the substrates: (a) C_f/Al composites; (b) TiAl alloys.

et al. (2002), Mukasyan and White (2007) and Feng et al. (2007) respectively joined superalloys, ceramics and cermet by SHS, which has verified its feasibility in joining field.

In previous work, Feng et al. (2016, 2017) joined the C_f/Al composites to TiAl alloys through directly SHS joining. But the brittle interfacial reaction products could not effectively relieve the joint stresses. This work is the extension of the previous work. These two materials were brazed using AgCu/TiZrNiCu filler metals. The AgCu filler metals were preferred to minimize the joint residual stresses through their plastic deformation. The laser-induced SHS reaction acted as an auxiliary heating source to rapidly melt the filler metals and realize the high-efficiency brazing process. The exothermic features of the Ni-Al-Zr interlayer and the joint microstructure were investigated. The relationship between joint microstructure and mechanical properties under different parameters were systemically studied.

2. Experimental procedure

The C_f/Al composites used in this study have a fiber volume fraction of 50% in a 6061 aluminum matrix. TiAl alloys have the nominal composition of Ti-48Al-7V-0.3Y (at.%). Fig. 1 shows the microstructure of the substrates in backscattered electron (BSEs) mode. Due to an addition of vanadium and yttrium, the TiAl alloys consist of γ phase (dark region), discontinuous retained B_2 (gray region) and YAl_x (bright region) phases. The C_f/Al and TiAl substrates were cut into pieces with the size of 5mm × 5mm × 3mm and 12mm × 8mm × 2mm, respectively. Prior to joining, all the joining surfaces were polished with SiC papers up to grit 1000, and cleaned ultrasonically in acetone for 15min to eliminate impurities.

Commercial powders (Beijing Xing Rong Yuan Technology Co., Let., China) of Ni (45 μm, 99.5%), Al (45 μm, 99.5%) and Ti (25 μm, 99.5%) were used for interlayers. Appropriate amounts of powders were weighed out in accord with the composition of Ni (65.08 wt.%), Al (29.92 wt.%) and Zr (5 wt.%), and milled in an agate bowl using Al_2O_3 balls for 1h in argon with the rotation speed of 300 rpm. The diameters of the agate bowl balls were 5 mm and 10 mm in diameter respectively. The weight ratio of Al_2O_3 ball to powders was 10:1. The milled powders weighted 0.5 g were uniaxially cold-pressured into cylindrical shape of 10 mm diameter and about 1.3 mm height. The green density of the powder compact was ~ 90% of the theoretical density under the pressure force of 50 kN.

Ag-28Cu (wt.%) foils with a thickness of 50 μm, 100 μm, 150 μm, and Ti-35Zr-15Ni-15Cu (wt.%) amorphous foils with a thickness of 40 μm were used as the filler metals. Fig. 2 shows the schematic diagram of the joining system. The powder compact and the filler metals were sandwiched between the substrates under a pressure (1–5 MPa) provided by a special fixture. The brazing couple had an order of C_f/Al/TiZrNiCu/AgCu/Ni-Al-Zr/ AgCu/TiZrNiCu/TiAl. The brazing proceeded in an inert, argon atmosphere. Laser beam (Ytterbium Fiber Laser, YLR-100-AC, beam power of 100W, beam diameter of 0.2mm) heated the compact for 5s, resulting in ignition and subsequent propagation of the exothermic reaction front through the composite, to finish the brazing.

The combustion temperature was measured employing a fine-wire (300μm) Pt/Pt-13%Rh thermocouple. The exothermic property of Ni-Al-Zr interlayer was examined by the differential scanning calorimetry (DSC, STA449F3). The interlayer products and brazed joint were examined by X-ray diffraction (XRD, D8 ADVANCE), transmission electron microscopy (TEM, Talos F200x) and scanning electron microscopy (SEM, Hitachi S-4700) equipped with energy dispersive spectrometer (EDS). The TEM specimens were prepared by the focused ion beam (FIB, Helios NanoLab 600i FIB/SEM). The joint shear strength at room temperature was achieved using the Instron-1186 universal testing machine at a shear rate of $0.5 mm \cdot min^{-1}$.

3. Results and discussion

3.1. Characterization of the Ni-Al-Zr interlayer

Considering its (i) low reaction activation energy, (ii) high exothermicity and (iii) combustion stability, equimolar Ni-Al system was selected as the exothermic interlayer in this study. A small amount (5 wt.%) of Zr (the strong carbide-forming element) was also added to enhance the interlayer's chemical affinity to the carbon fibers. The DSC analysis was carried out to characterize the exothermic reaction of the Ni-Al-Zr interlayer. Fig. 3(a) indicates that during the heating process, a sharp peak, corresponding to exothermic reaction (Ni + Al = NiAl, $\Delta H = -118.407 kJ\ mol^{-1}$), began to appear at the temperature of ~ 850 K and then reached the maximum value at 904.26 K.

In previous work, Feng et al. (2016) calculated the adiabatic temperature of Ni-Al-Zr reaction system. The Ni-Al-Zr interlayer used in this study processes an adiabatic temperature of 1912 K. Munir and Anselmi-Tamburini (1989) reported that 1800 K is the empirical lower limit adiabatic temperature for a self-sustaining exothermic reaction. The Ni-Al-Zr interlayer used in this study satisfied the empirical criterion. After the interlayer was ignited by laser beam, a stable combustion wave was observed. The corresponding temperature-time information was recorded simultaneously. The data in Fig. 3 (b) demonstrate a sharp temperature increase. Due to the unavoidable heat exchange with the surrounding environment, the peak temperature was lower than the theoretical adiabatic temperature. This obtained peak temperature was comparable to the results of a Ni-Al compact reported by Lin et al. (2013) and Thiers et al. (2002). The measured peak temperature (~1700 K) was much higher than the melting point of the AgCu filler metal (1053 K) and the TiZrNiCu filler metal (1043–1093 K), which means the exothermic reaction of Ni-Al-Zr interlayer can provide enough heat for the subsequent brazing process.

Fig. 4 displays the TEM micrographs of the interlayer products. The interlayer products consisted of three phases, i.e., the small island-like dark phase (A'), the offwhite block phase (C') and the remaining grey

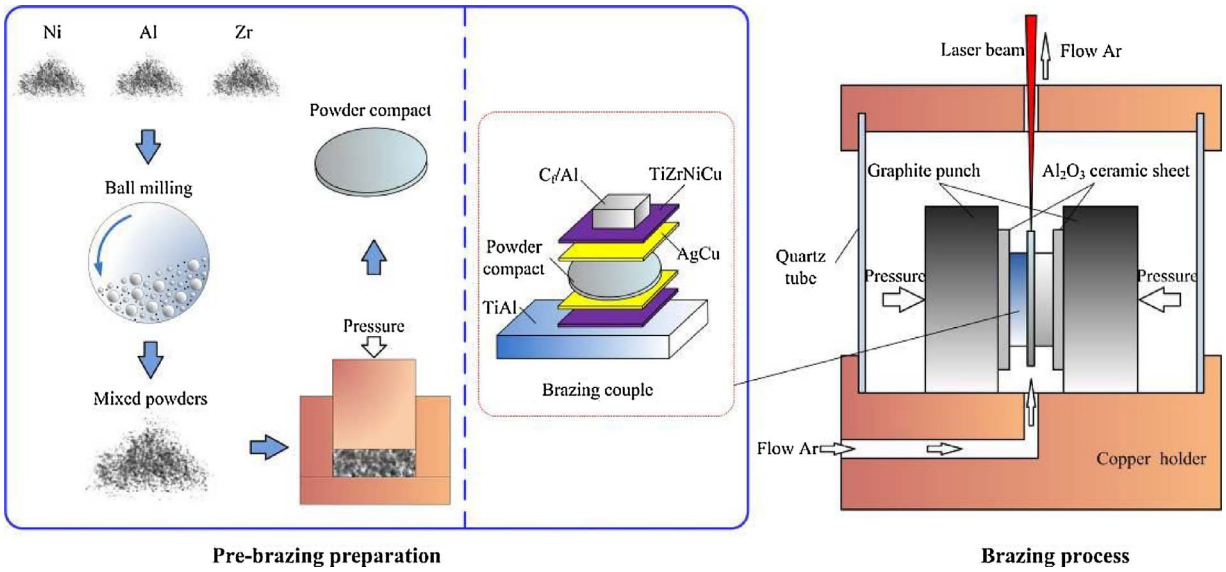

Fig. 2. Schematic of the brazing configuration.

phase (B'). The electron diffraction (SAED) data in Fig. 4(b)–(d) identify these phases. The island-like dark phase (A'), grey phase (B') and the offwhite block phase (C') were respectively confirmed as the Ni_2AlZr with ClCs-type crystal structure, $Ni_3Al_5Zr_2$ with $Mn_{23}Th_6$-type crystal structure and B_2-type NiAl. The XRD test was conducted on the interlayer products as well. Data in Fig. 4(e) reveal that NiAl and Ni-Al-Zr compounds were detected, which agrees with TEM results. The peaks appearing at $2\theta = 30.95°$, 44.34°, 55.04°, 64.49°, 81.60° and 97.97° were respectively confirmed as (100), (110), (111), (200), (211) and (220) of the NiAl phase, in accordance with the standard JCPDS card (No. 44-1188). Peaks appearing at $2\theta = 25.35°$, 41.74° and 76.37° were respectively confirmed as (111), (220) and (422) of the Ni_2AlZr phase, in accordance with the standard JCPDS card (No. 20-0037). Peaks appearing at $2\theta = 25.35°$, 38.82° and 41.74° were respectively confirmed as (222), (333) and (440) of the $Ni_3Al_5Zr_2$ phase, in accordance with the standard JCPDS card (No. 54-0437).

3.2. Microstructure

Fig. 5 represents the microstructure of the TiAl-C_f/Al brazed joint with AgCu/TiZrNiCu filler metals under 3 MPa. The joint was devoid of any defects such as cracks and voids. The Ni-Al-Zr interlayer reacted completely without any residual metal particles. The filler metals melted and infiltrated into the interlayer products, forming a mixture of dark block phase, grey reticular phase and the remaining white phase (see Fig. 5(d)).

To investigate the joint microstructure in detail, the magnified images of each domain are shown in Fig. 5(b)–(d). The corresponding EDS analysis on each marked location are shown in Table 1. Fig. (c) indicates that during the brazing, intensive interactions between the substrates, filler metal and Ni-Al-Zr interlayer, including dissolution, reaction and inter-diffusion, occurred, resulting in the formation of a continuous reaction layer (point A) on this side. According to the EDS results and report by Huneau et al, (1999), this reaction layer is Al_3NiTi_2 with the $MgZn_2$-type lattice structure. Cao et al. (2014) joined TiAl alloys to Ti_3AlC_2 ceramic and reported the formation of this reaction layer as well. The brazing seam consisted of reaction products of Ni-Al-Zr interlayer and filler metals. EDS results shows that dark phase (point B and D) is the NiAl phase (the Ni:Al atomic ratio of ~1:1). The white phase (point C) enriched in Ag was determined to be Ag(s,s) phase. The remaining grey phase (point E) mainly had the Ni, Al, Zr, Ti and Cu, and was speculated as a mixture of Ni-Al-Zr and Al-Cu-Ti compounds. The XRD test was carried out to further identify the phase composition. The C_f/Al substrate was removed by grinding until the brazing seam was reached. The sample was then subjected to XRD procedure. NiAl, Ag, Ni-Al-Zr and Al-Cu-Ti compounds were detected in Fig. 6, which confirmed the correctness of above expectation.

Fig. 5(b) represents the interface between the C_f/Al substrate and the brazing seam. Unlike the TiAl side, the C_f/Al/brazing seam interface didn't have a clear boundary. This is because the melting point of aluminum matrix is low (~930 K). Under the effect of exothermic reactions, the adjacent aluminum matrix melted, largely enhancing the elements diffusion in this region. The formed reaction products ((Zr,Ni,Ti)Al_3, point F) extended to the C_f/Al composites and

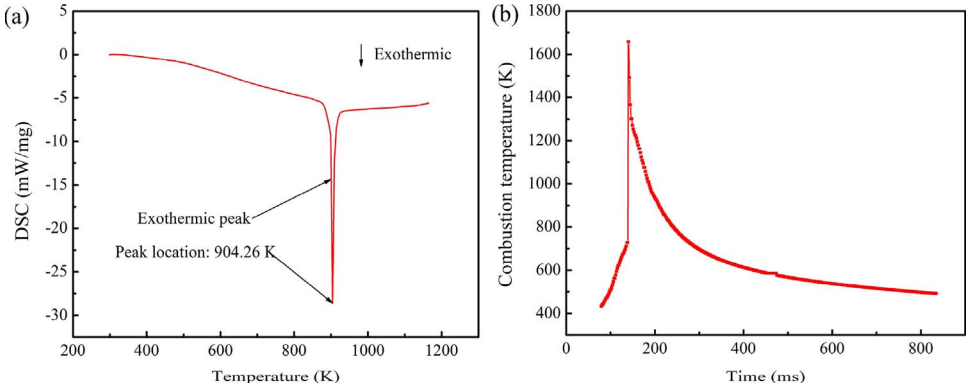

Fig. 3. (a) DSC curve of the Ni-Al-Zr interlayer; (b) combustion temperature of the Ni-Al-Zr interlayer.

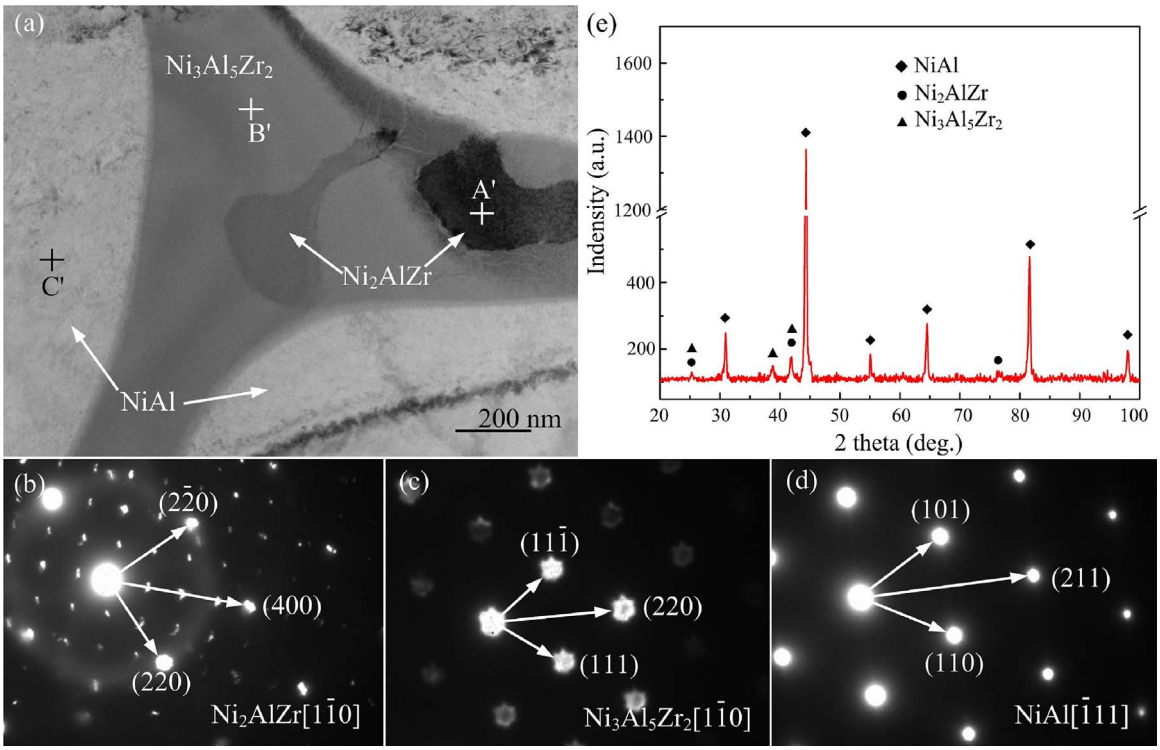

Fig. 4. (a)–(d) TEM micrographs and (e) XRD results of the Ni-Al-Zr interlayer products.

surrounded the carbon fibers. Fig. 7 gives the elemental distribution of the brazed joint. Ag, Cu, Zr, Ti and Ni all had a long diffusion distance within the aluminum matrix. Fig. 7(c) and (d) indicate that Zr had a uniform distribution in the brazing seam and Ti enriched at the substrates/brazing seam interfaces. Zr and Ti have a strong affinity to carbon ($Zr + C \rightarrow ZrC$, $\Delta G^\circ = -193.27\ kJ\ mol^{-1}$; $Ti + C \rightarrow TiC$, $\Delta G^\circ = -180.48\ kJ\ mol^{-1}$). Fig. 8(b) shows the element distribution at the carbon fiber/brazing seam interface (Fig. 8 (a), corresponds to the marked rectangular zone in Fig.5 (b)). Ti and Zr accumulated around the carbon fibers, forming a ~400 thick Ti and Zr rich layer. In previous work, Feng et al. (2016, 2017) reported that the addition of Ti or Zr led to a formation of Ti—C or Zr—C reaction layer at the interlayer/carbon fibers interface. The Ti and Zr rich layer in this study was speculated as a mixture of Zr—C and Ti—C compounds. The formation

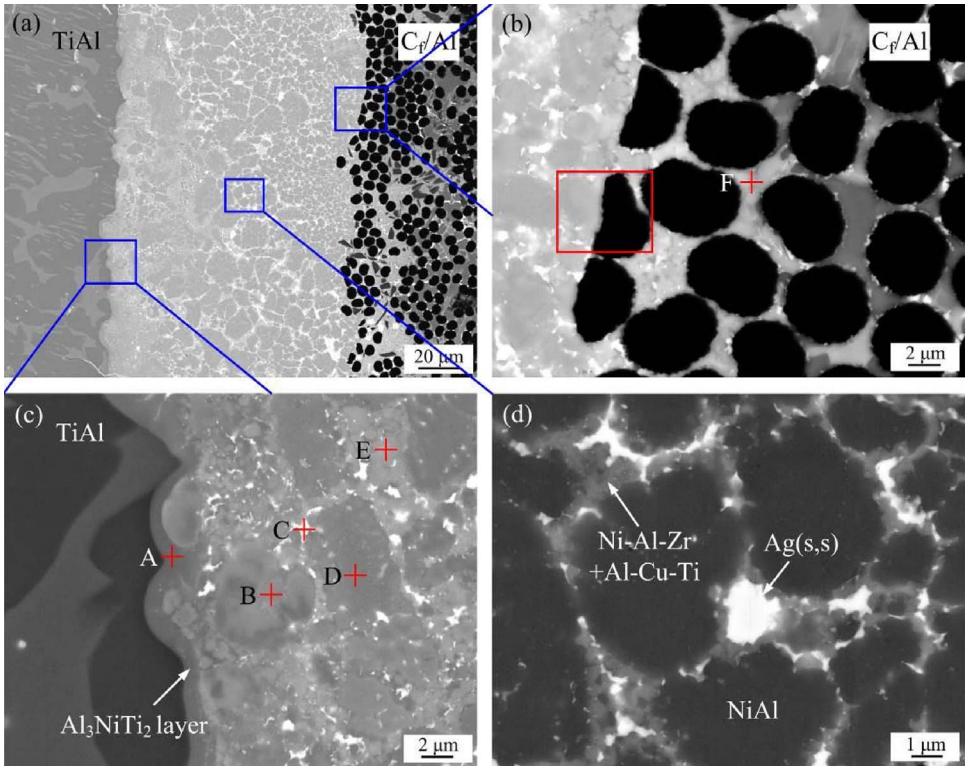

Fig. 5. Microstructure of the TiAl-C_f/Al joint. (a) Overall view; (b) the C_f/Al side; (c) the TiAl side; (d) the joint center.

Table 1
EDS results of the joint in Fig. 5.

Location	Elements (at.%)							Possible phase
	Ni	Al	Zr	Ti	V	Ag	Cu	
A	21.93	45.28	1.24	28.90	2.65	/	/	Al_3NiTi_2
B	55.86	43.16	0.25	0.65	/	/	0.08	NiAl
C	7.68	13.71	0.72	/	/	73.67	4.22	Ag(s,s)
D	48.21	51.32	0.26	0.22	/	/	/	NiAl
E	40.10	26.59	5.61	18.66	/	0.85	8.19	Ni-Al-Zr + Al-Cu-Ti
F	19.43	69.39	6.16	5.03	/	/	/	$(Ni,Ti,Zr)Al_3$

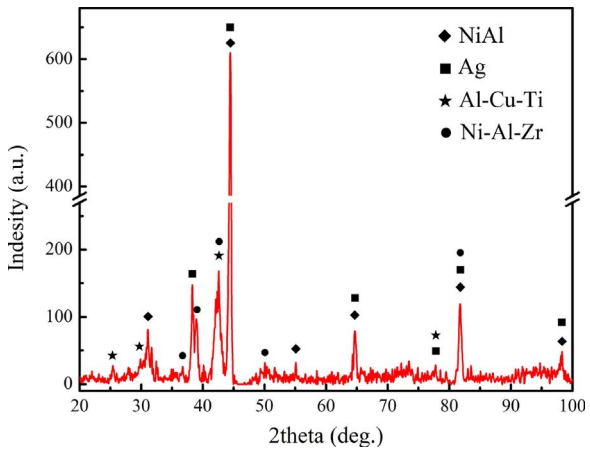

Fig. 6. XRD patterns of the brazing seam.

of this layer enhanced the wettability of filler metal on the carbon fibers, effectively improving the bonding quality between the C_f/Al composites and filler metals.

3.3. Effect of thickness of AgCu foils on the microstructure

Fig. 9 shows the interfacial microstructures of the brazed joints under 3 MPa. On each side, the thickness of TiZrNiCu foil was 40 μm. The thickness of AgCu foil was varied to investigate its effect on the joint microstructure. As shown in Fig. 9, when the AgCu foils became thicker, the joint domain underwent some obvious changes. Fig. 9 (c) indicates that without AgCu foils, the brazing seam consisted of NiAl and Ni-Al-Zr + Al-Cu-Ti. The application of AgCu foils produced some white Ag(s,s) phase around the NiAl phase. Increasing the thickness of AgCu foils resulted in a higher volume fraction of AgCu in the brazing system. More Ag(s,s) phases were formed during the brazing. Hence, the volume fraction of bright Ag(s,s) phase increased in the brazing seam, as illustrated in Fig. 9(f), (i) and (l).

The morphology of substrates/brazing seam interfaces also changed when varying the thickness of AgCu foils. Fig. 9(b), (e), (h) and (k) show that a thicker AgCu foil leads to a flatter TiAl/brazing seam interface, indicating the weakening tendency of the interfacial reactions in this region. The reason is hypothesized as follows. During the brazing, the AgCu foils located between the substrates and the interlayer, melted and absorbed a certain quantity of heat. The melted AgCu foils acted as a barrier to the heat transfer between the substrates and the interlayer. Thicker AgCu foils promoted this effect and decreased the heat absorbed by the substrates. As a result, the interfacial reactions were weakened, leading to a flatter interface. Fig. 9(a), (d), (g) and (j) represent the details at the TiAl/brazing seam interfaces. The thickness of the Al_3NiTi_2 reaction layer was 4.68 μm, 3.48 μm, 1.36 μm and < 0.5 μm respectively. Since the interfacial reaction is highly temperature dependent, the drop of Al_3NiTi_2 reaction layer thickness is expected to be the evidence of the decreased temperature at the substrates/filler metal interfaces.

3.4. Effect of brazing pressure on the microstructure

Fig. 10 displays the interfacial microstructures of the TiAl-C_f/Al joints brazed at different pressures. The thicknesses of AgCu foils and TiZrNiCu foils on each side were 100 μm and 40 μm respectively. The brazing pressure influenced the joint microstructure in two aspects: (i) the disappearance of pores and (ii) the distribution of white Ag(s,s) phase. When the brazing pressure was low, large quantity of pores were observed in the joint. The Ag(s,s) phase mainly accumulated in the region near the substrates, as shown in Fig. 10(a). Increasing brazing

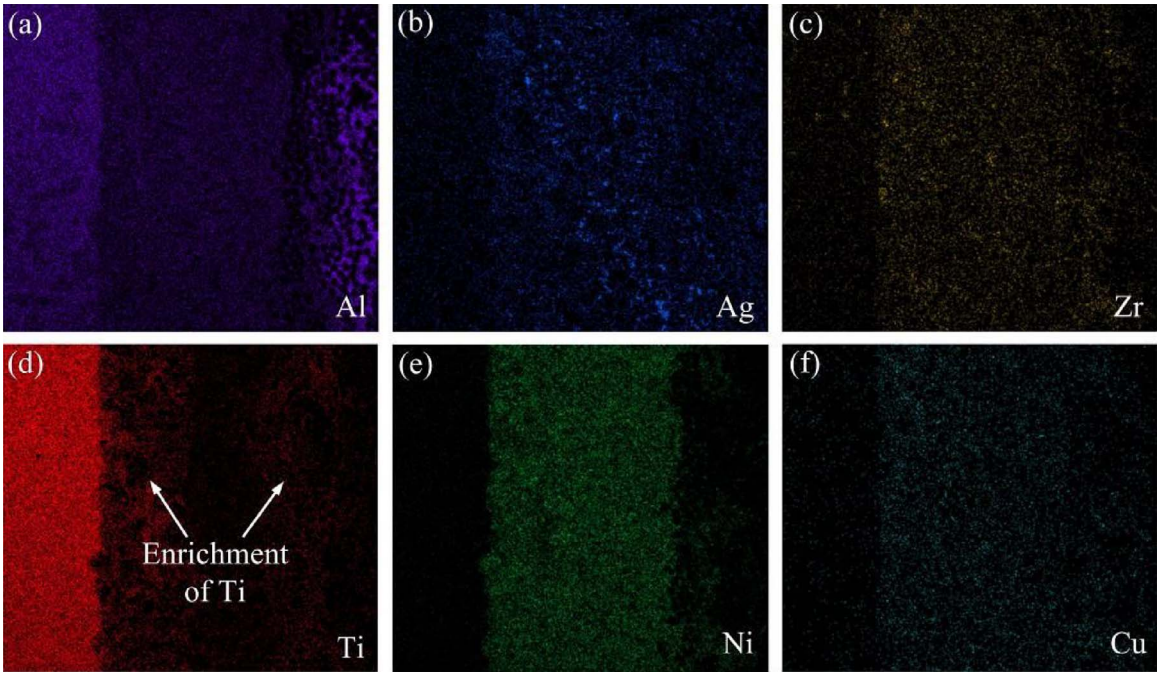

Fig. 7. (a)–(f) Element map of Al, Ag, Zr, Ti, Ni and Cu.

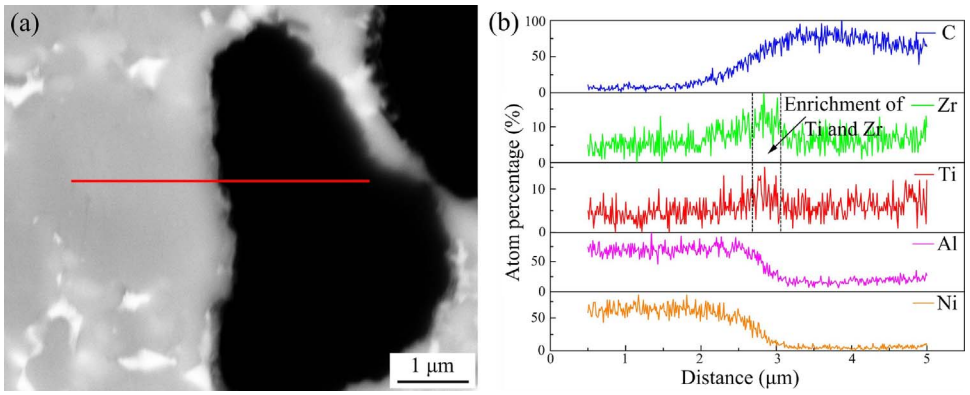

Fig. 8. (a) Interface between carbon fiber and reaction products; (b) element distribution of C, Zr, Ti, Al and Ni along the red line.

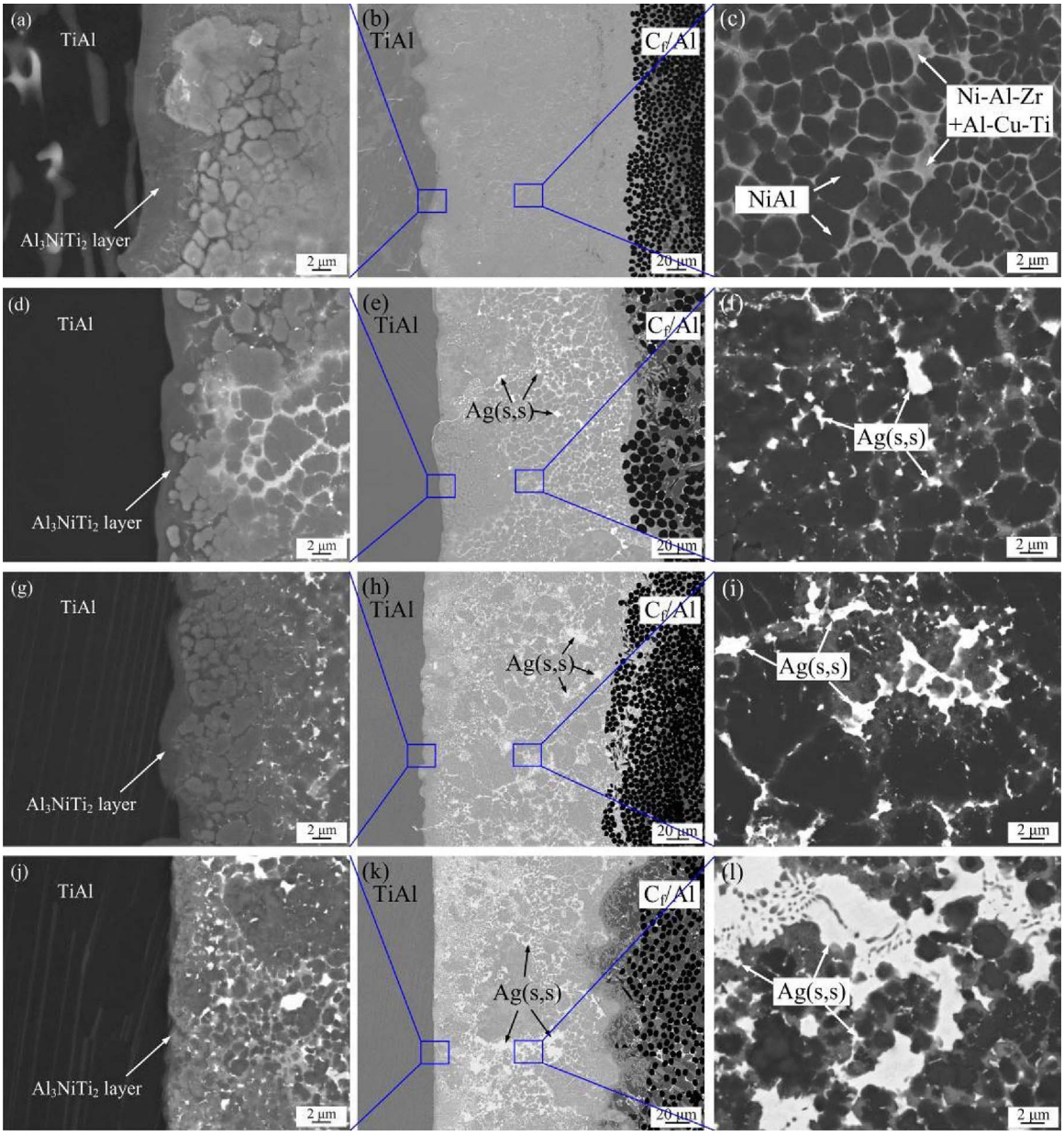

Fig. 9. Microstructures of the joints with the AgCu thickness of (b) 0 μm, (e) 50 μm, (h) 100 μm and (k) 150 μm, respectively.

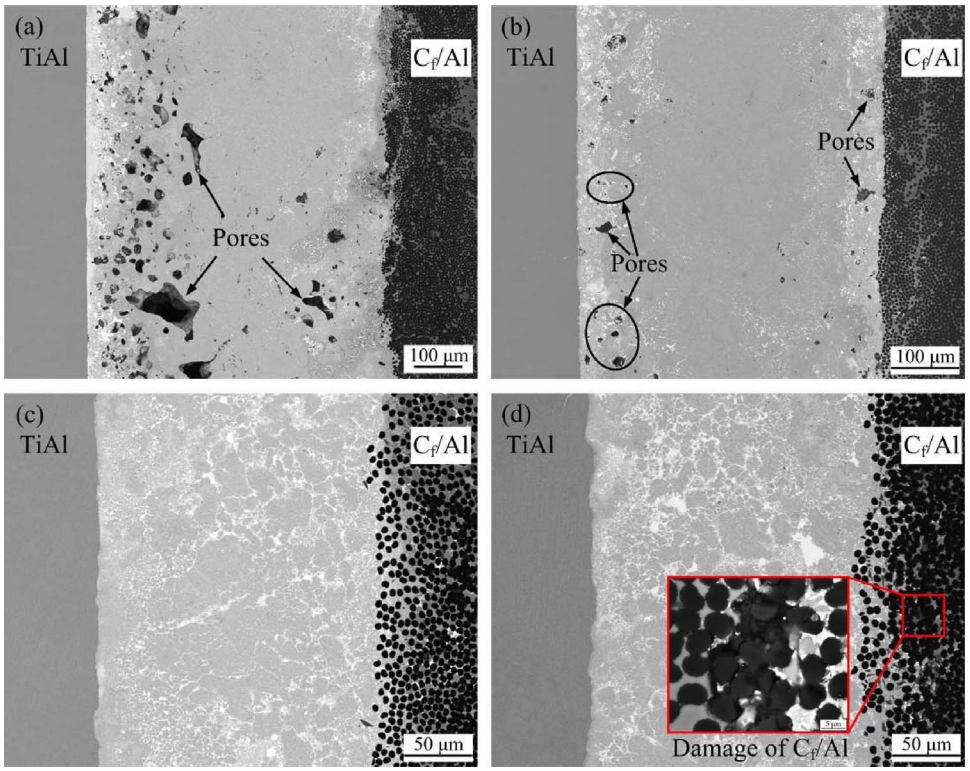

Fig. 10. Microstructures of the joints under different joining pressures. (a) 1 MPa; (b) 2 MPa; (c) 4 MPa; (d) 5 MPa.

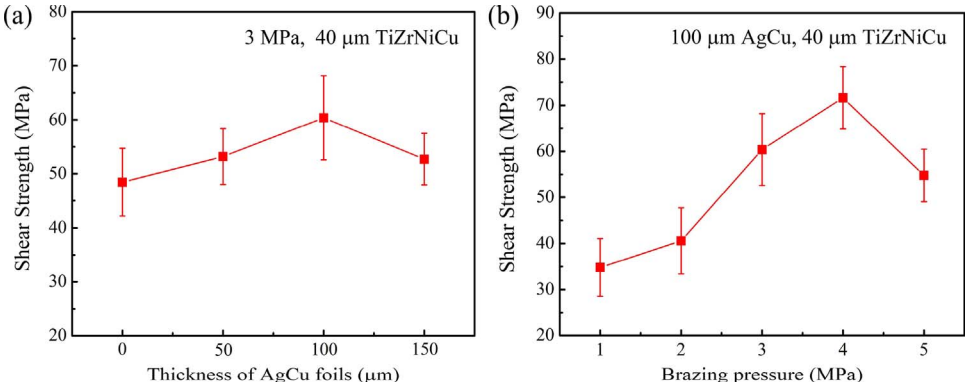

Fig. 11. Effect of (a) the thickness of AgCu foils and (b) the brazing pressure on the joints shear strength.

pressure decreased both the population of pores and their size. Meanwhile, the Ag(s,s) phase gradually moved towards the center of the brazing seam. When the brazing pressure reached 4 MPa, the joint was pore-free and the Ag(s,s) had an uniform distribution in the brazing seam.

During the brazing, violent exothermic reactions occurred in the Ni-Al-Zr interlayer. The filler metals and interlayer products were in a mushy, liquid-solid state. Applying brazing pressure led to an extrusion deformation of the reaction products, which helped eliminate the original pores in powder interlayer. Due to the cooling effect of adjacent substrates, the reaction products solidified quickly. Low pressure led to limited deformation in the joint and could not completely remove the pores. The filler metal could not fully infiltrate into the interlayer products. Higher pressure increased the extrusion deformation of the reaction products, enhancing the advection between the melting filler metals and interlayer products. The formed low-melting-point Al-Cu-Ti compounds and Ag(s,s) phases filled the pores more easily. Therefore, the pores in the brazing seam gradually disappeared as the brazing pressure increased. A pore-free joint with evenly distributed Ag (s,s) phases was achieved when the pressure was 4 MPa, as shown in Fig. 10(c). Further increase of the brazing pressure resulted in a large deformation of the C_f/Al due to the low-melting point of aluminum matrix. The enlargement in Fig. 11(d) shows that the connection between the aluminum matrix and carbon fibers was damaged. The bonding on the C_f/Al side was weakened.

3.5. Mechanical properties

The shear strength and the nano-indentation testing were performed at room temperature to establish the mechanical properties of different TiAl-C_f/Al brazed joints. Shear strength of the joints brazed under different conditions is presented in Fig. 11. The results of nano-indentation tests, which display the distribution of the hardness and elastic modulus of reaction phases across the joint, are shown in Fig. 12.

As shown in Fig. 11(a), when the thickness of AgCu foils increases, the shear strength gradually increases until the maximum shear strength of 60.4 MPa is reached, and then droppes down when the thickness of AgCu foils is 150 μm. The change of shear strength is strongly dependent on the microstructure evolution as follows from Fig. 9. Variation of the thickness of AgCu foils influenced the joint shear strength in two ways. First, varying the thickness of AgCu foils changed the volume fraction of Ag(s,s) phases in the brazing seam. When the C_f/

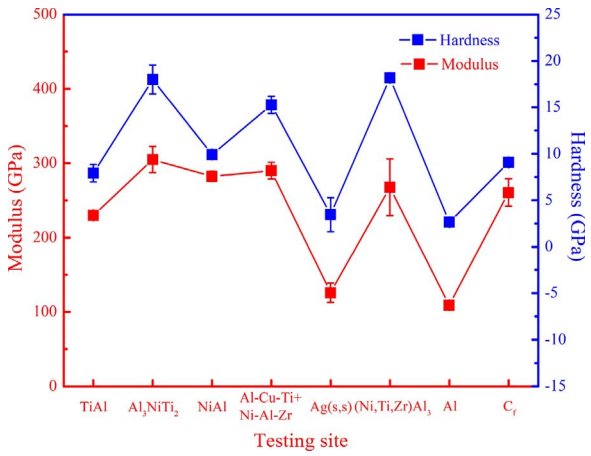

Fig. 12. Hardness and elastic modulus distribution across the joint interface.

Al composites and TiAl alloys were brazed with TiZrNiCu filler metals, the brazing seam was the reaction products of Ni-Al-Zr interlayer and TiZrNiCu filler metal. According to the Ni-Al-Zr and Al-Cu-Ti phase diagrams, the preferred products were NiAl intermetallics, Ni-Al-Zr and Al-Cu-Ti ternary compounds. The results of nano-indentation tests in Fig. 13 indicate that NiAl, Ni-Al-Zr + Al-Cu-Ti phases have the high elastic modulus (282.7 GPa, 290.4 GPa respectively) and hardness (9.9 GPa and 15.3 GPa respectively). Cai et al. (2016) indicated that reaction phases with higher hardness and elastic modulus exhibit a lower plastic deformation capability. Cao et al. (2017) suggested that the plastic deformation can release the residual stress in the joint, which is beneficial to the joint properties. Without AgCu foils, the brazing seam showed poor capability of plastic deformation, resulting in high residual stress in the joint and lowest shear strength. AgCu foils produced Ag(s,s) phases in the brazing seam. Ag(s,s) phase possesses a good capability of plastic deformation due to its low elastic modulus (125.8 GPa) and hardness (3.5 GPa). As the AgCu foils became thicker, the volume fraction of Ag(s,s) phase in the brazing seam featured a remarkable increase. Hence, more action of the shear forces could be absorbed. Second, varying the thickness of AgCu foils changed the thickness of the reaction layers on both sides. As analyzed in Section 3.3, thicker AgCu foils decreased the reaction heat absorption by the substrates, thus weakening the interfacial reactions. The thickness of Al_3NiTi_2 layer decreased from 4.7 μm to < 0.5 μm (see Fig. 9(a), (d), (g) and (j)). Thin reaction layer decreased the bonding quality on both sides. It should be noted that as the AgCu foils became thicker, there is a competitive relationship between the impacts of Ag(s,s) and reaction layer. The maximum shear strength is the result of a trade-off of these two factors. When the thickness of AgCu foils increased from 0 μm to 100 μm, the Ag(s,s) dominated the variation tendency of the joint shear strength. The elevated volume fraction of Ag(s,s) in the brazing seam effectively relieved the joint residual stress, resulting in the gradual elevation of the shear strength from 48.5 MPa to 60.4 MPa. When the thickness of AgCu foils further increased to 150 μm, the Al_3NiTi_2 reaction layer became < 0.5 μm and could not sustain a large force during the shear test. It severely affected the bonding quality and led to the decrease of the shear strength.

Fig. 11(b) represents the relationship between the brazing pressure and the joint shear strength. As the brazing pressure increases, the joint shear strength has a similar variation tendency with Fig. 11 (a). When the brazing pressure was 1 MPa, a large number of pores were produced in the brazing seam. They reduced the bonding area between the substrates and the interlayer products. Ag(s,s) concentrated near the substrates and could not effectively relieve the residual stress. The shear strength has the lowest value of 34.8 MPa. With the increase of the brazing pressure, both the population of pores and their size reduced remarkably. The Ag(s,s) phase gradually moved towards the center of the brazing seam and had a uniform distribution. During the brazing, the Ag(s,s) phase deformed plastically, largely relieving the joint residual stress. The joint shear strength slowly increased, reaching the maximum shear strength of 71.6 MPa when the brazing pressure was 4 MPa. Fig. 13 shows the joint fracture morphology. It demonstrates that the failure took place within the C_f/Al composites. The fractured carbon fibers were observed in the enlargement of the fractured surface. This indicates that the reaction products in the brazing seam were not the weakest part and the interfacial bonding was reliable. According to the Al—C phase diagram, Al can react with C, forming the Al_4C_3 compounds. In C_f/Al composites, the Al_4C_3 reaction layer is the medium connecting the aluminum matrix and carbon fibers. The further increase of the brazing pressure caused a large deformation within C_f/Al composites and damaged this brittle Al_4C_3 reaction layer. Microcracks occurred at the carbon fiber/aluminum matrix interface, see Fig. 10(d). The joint shear strength sharply declined to 54.8 MPa.

4. Conclusions

(1) The laser-induced SHS reaction of Ni-Al-Zr interlayer produced a mixture of NiAl, Ni_2AlZr and $Ni_3Al_5Zr_2$ compounds, and provided a local reaction temperature of ~1700 K. The representative interfacial structure of the brazed joint was TiAl/Al_3NiTi_2/NiAl + Ni-Al-Zr + Al-Cu-Ti + Ag(s,s)/ (Ni,Ti,Zr)Al_3/(C_f/Al).

(2) Zr and Ti accumulated around the carbon fibers and enhanced the bonding quality on the C_f/Al side. Varying the thickness of AgCu foils on each side and the brazing pressure changed the distribution of Ag(s,s) phase and pores in brazing seam as well as the interfacial reactions.

(3) When the thickness of AgCu foils was 100 μm and the brazing pressure was 4 MPa, the joint was free of pores and cracks. The joint shear strength under that condition reached the maximum value of 71.6 MPa.

Acknowledgements

The authors gratefully acknowledge the financial support from the

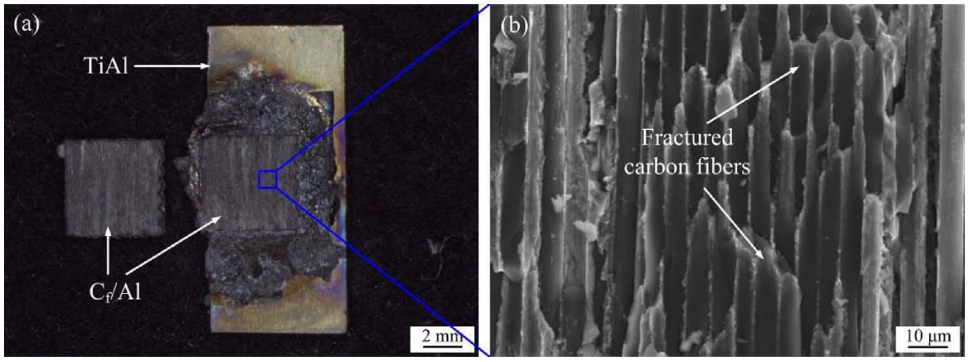

Fig. 13. Fracture of the joint. (a) Overall morphology; (b) fracture micro morphology.

National Natural Science Foundation of China under grant no. 51075101. Guangjie Feng acknowledges the support from the China Scholarship Council for 1 year's study at the University of Maryland, College Park. DPS acknowledges the support through the Distinguished 1000 Plan Foreign Professor appointment at the Harbin Institute of Technology, PR China.

References

Cao, J., He, P., Wang, M., 2011. Mechanical milling of Ti–Ni–Si filler metal for brazing TiAl intermetallics. Intermetallics 19, 855–859.

Cao, J., Liu, J., Song, X., Lin, X., Feng, J., 2014. Diffusion bonding of TiAl intermetallic and Ti_3AlC_2 ceramic: interfacial microstructure and joining properties. Mater. Des. 56, 115–121.

Cao, J., Dai, X., Liu, J., Si, X., Feng, J., 2017. Relationship between microstructure and mechanical properties of TiAl/Ti_2AlNb joint brazed using Ti-27Co eutectic filler metal. Mater. Des. 121, 176–184.

Cai, X.Q., Wang, Y., Yang, Z.W., Wang, D.P., Liu, Y.C., 2016. Transient liquid phase (TLP) bonding of Ti_2AlNb alloy using Ti/Ni interlayer: microstructure characterization and mechanical properties. J. Alloys Compd. 679, 9–17.

Cheng, L., Li, J., Xue, X., Tang, B., Kou, H., Bouzy, E., 2016. General features of high temperature deformation kinetics for γ-TiAl-based alloys with DP/NG microstructures: part I. A survey of mechanical data and development of unified rate-equations. Mater. Sci. Eng. A 678, 389–401.

Dai, X., Cao, J., Liu, J., Su, S., Feng, J., 2015. Effect of holding time on microstructure and mechanical properties of ZrO_2/TiAl joints brazed by Ag–Cu filler metal. Mater. Des. 87, 53–59.

Feng, G., Li, Z., Zhou, Z., Wang, Y., 2016. Joining of C_f/Al composites and TiAl intermetallics by laser-induced self-propagating high-temperature synthesis using the Ni-Al-Zr interlayer. Mater. Des. 110, 130–137.

Feng, G., Li, Z., Jacob, R.J., Yang, Y., Wang, Y., Zhou, Z., Sekulic, D.P., Zachariah, M.R., 2017. Laser-induced exothermic bonding of carbon fiber/Al composites and TiAl alloys. Mater. Des. (126), 197–206.

Feng, G.J., Li, Z.R., Feng, S.C., Zhang, W.J., 2015a. Microstructure evolution and formation mechanism of laser-ignited SHS joining between C_f/Al composites and TiAl alloys with Ni–Al–Ti interlayer. Rare Met. 36, 746–752.

Feng, G.J., Li, Z.R., Liu, R.H., Feng, S.C., 2015b. Effects of joining conditions on microstructure and mechanical properties of C_f/Al composites and TiAl alloy combustion synthesis joints. Acta Metall. Sin. (Engl. Lett.) 28, 405–413.

Feng, G., Li, Z., Feng, S., Shen, Z., 2015c. Effect of Ti–Al content on microstructure and mechanical properties of C_f/Al and TiAl joint by laser ignited self-propagating high-temperature synthesis. Trans. Nonferrous Met. Soc. China 25, 1468–1477.

Feng, J.C., Cao, J., Li, Z.R., 2007. Microstructure evolution and reaction mechanism during reactive joining of TiAl intermetallic to TiC cermet using Ti–Al–C–Ni interlayer. J. Alloys Compd. 436, 298–302.

Huneau, B., Rogl, P., Zeng, K., Schmid-Fetzer, R., Bohn, M., Bauer, J., 1999. The ternary system Al–Ni–Ti part I: isothermal section at 900 °C; Experimental investigation and thermodynamic calculation. Intermetallics 7, 1337–1345.

Li, J., Liu, L., Wu, Y., Zhang, W., Hu, W., 2008. A high temperature Ti–Si eutectic braze for joining SiC. Mater. Lett. 62, 3135–3138.

Li, Z., Feng, G., Wang, S., Feng, S., 2016. High-efficiency joining of C_f/al composites and TiAl alloys under the heat effect of laser-ignited self-propagating high-temperature synthesis. J. Mater. Sci. Technol. 32, 1111–1116.

Li, Z.R., Feng, G.J., Xu, K., Zhang, X.L., 2015. Microstructure and formation mechanism of SHS joining between C_f/Al composites and TiAl intermetallic with Al–Ni–CuO interlayer. Rare Met. 34, 17–21.

Lin, Y.C., Nepapushev, A.A., McGinn, P.J., Rogachev, A.S., Mukasyan, A.S., 2013. Combustion joining of carbon/carbon composites by a reactive mixture of titanium and mechanically activated nickel/aluminum powders. Ceram. Int. 39, 7499–7505.

Mukasyan, A.S., White, J.D.E., 2007. Combustion joining of refractory materials. Int. J. Self-Propagat. High.-Temp. Synth. 16, 154–168.

Munir, Z.A., Anselmi-Tamburini, U., 1989. Self-propagating exothermic reactions: the synthesis of high-temperature materials by combustion. Mater. Sci. Rep. 3, 277–365.

Pai, A., Sharma, S.S., D'Silva, R.E., Nikhil, R.G., 2015. Effect of graphite and granite dust particulates as micro-fillers on tribological performance of Al 6061-T6 hybrid composites. Tribol. Int. 92, 462–471.

Pascal, C., Marin-Ayral, R.M., Tedenac, J.C., 2002. Joining of nickel monoaluminide to a superalloy substrate by high pressure self-propagating high-temperature synthesis. J. Alloys Compd. 337, 221–225.

Shiue, R.K., Wu, S.K., Chen, S.Y., 2003. Infrared brazing of TiAl intermetallic using BAg-8 braze alloy. Acta Mater. 51, 1991–2004.

Song, X., Ben, B., Hu, S., Feng, J., Tang, D., 2017. Vacuum brazing high Nb-containing TiAl alloy to Ti60 alloy using Ti-28Ni eutectic brazing alloy. J. Alloys Compd. 692, 485–491.

Thiers, L., Mukasyan, A.S., Varma, A., 2002. Thermal explosion in Ni-Al system: influence of reaction medium microstructure. Combust. Flame 131, 198–209.

Velamati, M., Aguilar, E., Garza-Castañon, M.A., Hung, N.P., Powers, M., 2012. Laser and resistance joining of aluminum–graphite composite. J. Mater. Process. Technol. 212, 2549–2557.

Zhao, K., Liu, Y., Huang, L., Liu, B., He, Y., 2016. Diffusion bonding of Ti-45Al-7Nb-0.3W alloy by spark plasma sintering. J. Mater. Process. Technol. 230, 272–279.